Title
Thin anisotropic metasurfaces for simultaneous light focusing and polarization manipulation

Journal
Journal of the Optical Society of America B: Optical Physics, 32(2)

ISSN
0740-3224

Authors
Veysi, M
Guclu, C
Boyraz, O
et al.

Publication Date
2015-02-01

DOI
10.1364/JOSAB.32.000318

Peer reviewed

Thin anisotropic metasurfaces for simultaneous light focusing and polarization manipulation

Mehdi Veysi, Caner Guclu, Ozdal Boyraz, and Filippo Capolino*

Department of Electrical Engineering and Computer Science, University of California, Irvine, California 92697, USA
**Corresponding author: f.capolino@uci.edu*

Received August 27, 2014; revised November 16, 2014; accepted November 17, 2014;
posted December 17, 2014 (Doc. ID 221794); published January 22, 2015

The possibility of integration of two important categories of optical components, i.e., circular polarizer and lens, into a thin plasmonic metasurface is examined, for the realistic case when metal losses cannot be neglected, for example when operating in the visible spectrum, or at infrared when non-noble metals are used. We introduce a metasurface made of nanoantennas that offer enough degrees of freedom to control both amplitude and phase of the reflection coefficient. First a theoretical formulation is developed and then an optimal design for a polarizing lens at mid-infrared wavelengths near 4.3 μm is presented. A two-dimensional array of Y-shaped nanoantennas with polarization-dependent and spatially varying phase response offers the possibility of balancing the losses experienced by the x- and y-polarized incident fields and is the basis for such a compact polarizing lens.

OCIS codes: (160.3918) Metamaterials; (250.5403) Plasmonics; (050.6624) Subwavelength structures.
http://dx.doi.org/10.1364/JOSAB.32.000318

1. INTRODUCTION

Conventional optical devices such as lenses with aberration correction, and quarter-wave plates made of birefringent and chiral materials met the performance demand in both bandwidth and efficiency, but they are usually bulky, expensive, and difficult to fabricate and to integrate in nanophotonic systems. Nevertheless, applications demand cheaper and thinner devices with better performance. Over the last decade, space-variant dielectric gratings [1,2], and subwavelength thick plasmonic metasurfaces (MSs) have attracted increasing attention in modern optics and photonics due to their capability to introduce phase change discontinuities over subwavelength distances [3–8]. Techniques of beam shaping through phase discontinuities achieved by collections of resonant antennas have been used at centimeter and millimeter waves for a few decades [9]. This idea, applied to visible/infrared frequencies, can eliminate the need for propagation path compensation in lensing [10–15], or reduce the physical dimensions required for a quarter-wave plate [16–18]. Since the circular polarizer and lens are at the heart of many optical systems, the possibility of having both light focusing and polarization manipulation capabilities with a thin single layer plasmonic MS would significantly reduce the cost, volume, optical loss, and system complexity.

Recently, single [19] and multilayer [20] MSs, made of Au layers with negligible losses, have been introduced at mid-infrared frequencies for both phase and polarization control. However, in various cases, especially at infrared and optical frequencies, materials have unavoidable losses, which need to be carefully addressed in order to ensure a practical design. In general, in mid-infrared and far-infrared regimes, the variations in the amplitude of the reflection/transmission coefficient with respect to the nanoantenna design parameters are negligible when low-loss metals, such as Au and Ag, are used. In this case, one needs to account only for the phase of the reflection/transmission coefficient. However, since Au and Ag are lossy at the visible and near-infrared regime, the amplitude of the reflection/transmission coefficient significantly changes with the nanoantenna design parameters. So, the synthesis of the polarizing lens at the visible/infrared regime is not in general a phase-only synthesis method and one should carefully consider both the amplitude and phase of the reflected/transmitted wave at the MS.

In this paper, we develop a phase-amplitude synthesis method for the polarizing lens design, when metal losses cannot be neglected. The first challenge is to find an appropriate nanoantenna which can simultaneously satisfy both a wide reflection phase range and polarization conversion. Hence, an anisotropic nanoantenna, which allows for independent tuning of the phase changes experienced by the x- and y-pol. incident fields, is needed. We show a novel single-layer metalens design based on Y-shaped nanoantennas capable of focusing and polarization manipulation, simultaneously. The theory and the example developed here will enable improvement of several devices, such as (i) reflecting or (ii) transmitting focusing lenses; (iii) polarizing lenses; (iv) lenses with dual foci, one for each polarization; and (v) lenses with dual foci, one for each wavelength. We show that anisotropic Y-shaped nanoantennas possess an additional degree of freedom compared to the other nanoantennas studied in the literature, such as V-shaped [3,4], cross-shaped, and rectangular-shaped ones [21]. Such an extra degree of freedom in Y-shaped nanoantennas gives rise to the possibility of balancing the losses experienced by the two orthogonally polarized incident fields that eventually improves the performance of the polarizing lens. In this paper, nanoantennas are assumed to be made of low-cost aluminum with non-negligible loss at mid-infrared to account for the loss in the design process. Although, we focus on the reflection-type geometry due to its high focusing [12,13] and

polarization conversion efficiencies [22], the theory and application of Y-nanoantennas can be straightforwardly extended to the transmission-type geometry.

2. THEORY

The proposed polarizing lens design consists of an array of Y-shaped nanoantennas patterned on one side of a dielectric layer deposited onto a metallic ground plane, as illustrated in Fig. 1. The MS is in the x–y plane, and it is illuminated by a normally incident slant-polarized plane wave whose transverse-to-z electric field phasor is $\mathbf{E}_t^i = E_0(\hat{\mathbf{x}}\cos\varphi_i + \hat{\mathbf{y}}\sin\varphi_i)e^{jkz}$, where E_0 is its magnitude, k is the free-space wavenumber, and φ_i is the angle of the electric field vector with respect to the x axis (in the following we assume a $e^{j\omega t}$ time-harmonic convention with ω the angular frequency). Here vectors are denoted by bold fonts and unit vectors are denoted by a hat. The transverse-to-z electric field phasor of the wave normally reflected by the polarizing lens is

$$\mathbf{E}_t^r = E_1\left(\hat{\mathbf{x}} + \frac{|\Gamma_y|}{|\Gamma_x|}e^{j(\phi_y-\phi_x)}\tan\varphi_i\hat{\mathbf{y}}\right),$$
$$E_1 = E_0|\Gamma_x|\cos\varphi_i e^{-jkz}e^{j\phi_x}, \tag{1}$$

where $\Gamma_{x,y} = |\Gamma_{x,y}|e^{j\phi_{x,y}}$ is the reflection coefficient pertaining to the x- and y-pol. components, respectively. In order to change the polarization state of the incident wave, we consider here a plasmonic MS made of anisotropic Y-shaped nanoantennas able to manipulate both Γ_x and Γ_y. At a certain wavelength such that the phase difference between the y- and x-pol. reflection coefficients, $(\phi_y - \phi_x)$, is 90° and the ratio of the wave reflection magnitude for the y-pol. to that of x-pol. is almost constant, $|\Gamma_y|/|\Gamma_x| = \cot\varphi_i$, the reflected wave is purely left-hand circularly polarized (LHCP). It is purely right-hand circularly polarized (RHCP) when $(\phi_y - \phi_x) = -90°$. Although the above conclusions have been derived for waves normally reflected from the MS, they are still reasonably valid for reflected waves with small oblique reflection angles (usually less than 30°–40° [23,24]).

For a general case, consider an oblique incident ray tube as in Fig. 1, propagating with a wave vector, $\mathbf{k}^i$, impinging on the MS and experiencing reflection. The direction of the reflected wave can be controlled based on the generalized Fermat principle [1–3,9] by a proper gradient of the phase of the reflection coefficient. Therefore the reflected beam can be steered

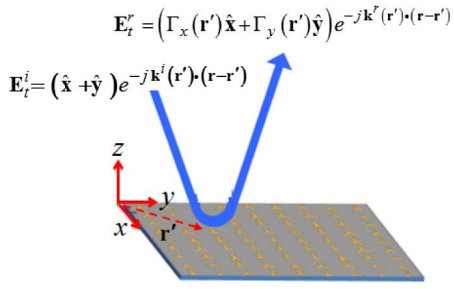

Fig. 1. Schematic of a MS composed of Y-shaped nanoantennas illuminated by a plane wave with transverse electric fields shown. The blue line represents a typical incident ray that is locally bended by the MS at a designed angle. The direction of the reflected wave vector, $\mathbf{k}^r = \mathbf{k}_t^r + k_z^r\hat{\mathbf{z}}$, depends on the phase of x-pol. and y-pol. reflection coefficients.

toward a desired direction $\mathbf{k}^r$ given by $\mathbf{k}_t^r - \mathbf{k}_t^i = (\partial\phi/\partial x)\hat{\mathbf{x}} + (\partial\phi/\partial y)\hat{\mathbf{y}}$, where $\mathbf{k}_t^i$ and $\mathbf{k}_t^r$ are, respectively, the transverse-to-z wave vectors of the incident and reflected fields and $\partial\phi/\partial i = \partial\phi_x/\partial i = \partial\phi_y/\partial i$, $i = x, y$ (note that $\partial\phi_x/\partial i = \partial\phi_y/\partial i$ is straightforwardly obtained by taking the derivative of the polarization conversion condition $(\phi_y - \phi_x) = \pm 90°$). The local values of phase and magnitude of the reflection coefficient are controlled by a proper choice of the unit cell elements of the MS. The elements should be modulated along the MS to provide the required gradient of the phase ϕ to achieve focusing. In the following element locations are denoted with $\mathbf{r}^{mn} = \mathbf{r}^{00} + ma\hat{\mathbf{x}} + nb\hat{\mathbf{y}}$, where m and n are integers, and a and b are the local periods along x and y.

Considering the generalized Fermat principle with the discretized MS unit cells, the phase of the reflection coefficient is changed adiabatically along the MS according to the expression

$$\mathbf{k}_t^r = \mathbf{k}_t^i + \left(\frac{\phi^{mn} - \phi^{(m-1)n}}{a}\right)\hat{\mathbf{x}} + \left(\frac{\phi^{mn} - \phi^{m(n-1)}}{b}\right)\hat{\mathbf{y}} \tag{2}$$

in order to bend the corresponding ray toward a certain direction $\mathbf{k}^r$. The above procedure is repeated for all other unit cells on the MS and the required phase of the reflection coefficient is found for each element. It is a common procedure to calculate the required reflection coefficient associated to a certain MS unit cell by assuming the MS periodic. This procedure provides accurate results if unit cells change gradually over the MS [9,14,25]. If all rays are focused at a certain focal point $\mathbf{r}_f$ the required phase of the reflection coefficient ϕ^{mn} at the mnth MS unit cell is found to be [9]

$$\phi^{mn} - [k_0|\mathbf{r}^{mn} - \mathbf{r}_f| + \mathbf{r}^{mn}.\ \mathbf{k}^i] = 2s\pi + \psi, \quad s = 0, \pm 1, \ldots. \tag{3}$$

Here, ψ is an arbitrary phase constant, and the subscripts x and y have been dropped since this equation applies to both polarizations. In summary, the focusing and polarization conversion mechanism of the anisotropic plasmonic metalens under the linearly polarized wave is conceptually described by Eqs. (1) and (3), where two approximations extensively used in reflectarray research have been applied [9,14,25]: (i) the concept of local periodicity, and (ii) the reflected phases $\phi_{x,y}^{mn}$ are evaluated at normal incidence. The latter approximation has been considered to be accurate especially for small to moderate incidence angles and focal length to diameter ratio larger than unity (in our case $f/D = 1.25$).

Note that all possible polarizations [linearly polarized (LP), RHCP, and LHCP] can be achieved by also adjusting the φ_i angle. To independently vary the reflection phases $\phi_{x,y}$ and amplitudes $|\Gamma_{x,y}|$ of each principle polarization of the incident wave, along the x and y directions, each unit cell should possess enough degrees of freedom. Hence, a Y-shaped nanoantenna shown in Fig. 2(a), recently used for thermal tuning the resonances of mid-infrared (IR) plasmonic antennas [28], is utilized as a unit cell. Its symmetric and asymmetric current modes are depicted in Fig. 2(a). Varying Δ and ℓ_1 leads to changes in both the x- and y-directed current paths. Note that ℓ_2 affects only the extension of the y-directed surface current path and has a negligible effect on the asymmetric mode. In the design, first, the two physical parameters of the Y-shaped

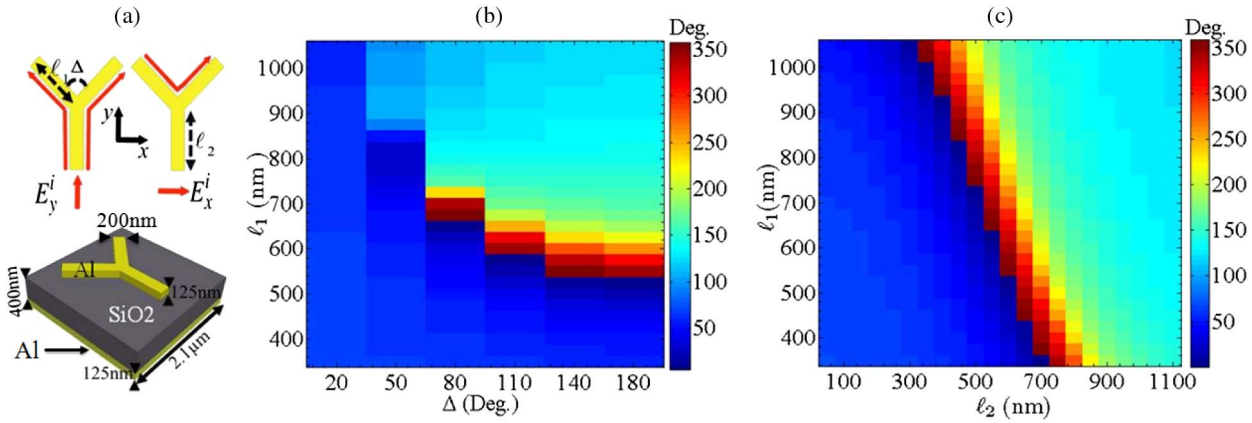

Fig. 2. (a) Schematic of a MS Y-shaped nanoantenna together with its current distribution for symmetric (top left) and asymmetric modes (top right), and the 3D view of each MS cell (bottom). (b) The reflection phase of the asymmetric mode for a MS made of identical Y-shaped nanoantennas at 4.3 μm as a function of the arm length, and the angle between the two arms, Δ, for $\ell_2 = 50$ nm. Although results are not plotted here, a similar trend is observed for other values of the stub length ℓ_2 ranging from 50 to 1100 nm. (c) The reflection phase of symmetric mode for a MS made of identical Y-shaped nanoantennas at 4.3 μm as a function of the arm length, and stub length, for $\Delta = 110°$. The lateral width and thickness of each arm are fixed at 200 and 125 nm, respectively. The complex relative permittivities of the Al and SiO_2 at 4.3 μm are −1601.3–j609.4 [26] and 1.9 – j0.018 [27], respectively.

elements, arm length ℓ_1 and arm angle Δ, are tuned to satisfy the focusing condition in Eq. (3) for the x-pol. incident wave at each mnth location on the MS as

$$\mathrm{err}_{(1)}^{mn}(\Delta,\ell_1) = |\phi_x^{mn} - \phi_x^{\mathrm{simulated}}(\Delta,\ell_1)|. \tag{4}$$

Here $\phi_x^{\mathrm{simulated}}$ is phase of the reflected x-pol. at the design wavelength λ, obtained from a simulation with the geometrical parameters optimized to meet the required ϕ_x^{mn} from Eq. (3). The elements are optimized using the frequency domain finite-element method (FEM) (provided by HFSS by Ansys Inc.) in a fully periodic arrangement (based on local periodicity assumption). To achieve circularly polarized focused beam upon reflection, it is necessary to tailor both the spatial phase and amplitude distributions of the reflected field by tuning each element on the MS. Therefore, the stub length ℓ_2 is then tuned to meet the proper condition for converting the polarization from linear to circular and to meet the focusing condition in Eq. (3) also for the y-pol. Note that tuning the stub length ℓ_2 has a negligible effect on the asymmetric mode of the Y-shaped elements and thus on the x-pol. focusing. Therefore, a second error function is defined based on the axial ratio (AR) of the reflected wave as

$$\mathrm{err}_{(2)}^{mn}(\Delta,\ell_1,\ell_2) = |\pm 1 - \mathrm{AR}(\Delta,\ell_1,\ell_2)|, \tag{5}$$

where plus or minus sign stands for a desired LHCP or RHCP, respectively. The AR depends on the physical parameters of the elements and is expressed as

$$\mathrm{AR}(\Delta,\ell_1,\ell_2) = -\frac{|E_R(\Delta,\ell_1,\ell_2)| + |E_L(\Delta,\ell_1,\ell_2)|}{|E_R(\Delta,\ell_1,\ell_2)| - |E_L(\Delta,\ell_1,\ell_2)|}, \tag{6}$$

where E_R and E_L are projections of the reflected electric field $\mathbf{E}_t^r$ [see Eq. (1)] onto the RHCP and LHCP unit vectors $\hat{\mathbf{e}}_R = (\hat{\mathbf{x}} - j\hat{\mathbf{y}})/\sqrt{2}$ and $\hat{\mathbf{e}}_L = (\hat{\mathbf{x}} + j\hat{\mathbf{y}})/\sqrt{2}$, respectively. The AR can be rewritten in terms of linear components as [29]

$$\mathrm{AR}(\Delta,\ell_1,\ell_2) = \mathrm{sgn}(\phi_y - \phi_x)\frac{\sqrt{|E_x|^2 + |E_y|^2 + E'}}{\sqrt{|E_x|^2 + |E_y|^2 - E'}}$$
$$E' = \sqrt{|E_x|^4 + |E_y|^4 + 2|E_x|^2|E_y|^2\cos(2(\phi_y - \phi_x))}, \tag{7}$$

where $E_{x,y} = |E_{x,y}|e^{j\phi_{x,y}}$ are the x- and y-pol. components of $\mathbf{E}_t^r$ [see Eq. (1)]. Note that for each MS element the phase difference $|\phi_x^{mn} - \phi_y^{mn}|$ between the x- and y-pol. reflection coefficients is set very close to 90° when minimizing $\mathrm{err}_{(2)}^{mn}$ in Eq. (5). Therefore, the focusing condition for ϕ_y^{mn} in Eq. (3) is automatically satisfied provided that ϕ_x^{mn} satisfies it, as already imposed by Eq. (4).

3. PARAMETRIC STUDY OF A METASURFACE MADE OF Y-SHAPED NANOANTENNAS

The range of phases of the x- and y-pol. reflection coefficients for a MS made of identical aluminum (Al) Y-shaped nanoantennas as a function of the physical parameters (arm length, stub length, and arm angle) at $\lambda = 4.3$ μm are shown in Figs. 2(b) and 2(c). It is observed that the 360° phase range required for the full control of the wavefront of the reflected wave is achieved. The low-loss silica substrate with low dielectric constant ($\varepsilon_r = 1.9$ at $\lambda = 4.3$ μm) is chosen here instead of higher dielectric constant substrates such as silicon to increase the MS bandwidth and at the same time decrease the rate of variation of reflection phase with the Y-shaped nanoantenna dimensions. The latter effect results in a lower sensitivity to manufacturing tolerances [9].

The phase difference between the x- and y-pol. reflection coefficients versus the arm length, ℓ_1, for different stub lengths, ℓ_2, is plotted in Fig. 3(a). As the stub length, ℓ_2, increases, the resonant length of the symmetric mode (y-directed current mode) increases, while the resonant length of the asymmetric mode (x-directed current mode) remains unchanged. Thus, for a given arm length, the phase difference between the x- and y-pol. reflection coefficients

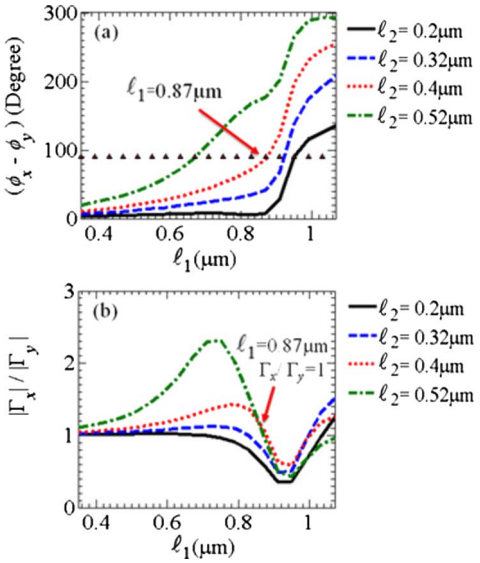

Fig. 3. (a) The effect of stub length on the phase difference between the x-pol. and y-pol. reflection coefficients. The horizontal line shows the 90° phase difference between the x-pol. and y-pol. reflection coefficients. (b) The effect of stub length on the amplitude ratio of the x-pol. to y-pol. reflection coefficient. The arm angle, Δ, is fixed at 50°.

increases as the stub length increases [see Fig. 3(a)]. Figure 3(b) also shows the amplitude ratio of the x-pol. to the y-pol. reflection coefficient versus the arm length, ℓ_1, for different stub lengths, ℓ_2. For $\ell_2 = 0.4$ μm and $\ell_1 = 0.87$ μm, the amplitude ratio of the x-pol. to the y-pol. reflection coefficient is equal to 1 and the phase difference between the x- and y-pol. reflection coefficients is 90° (see Fig. 3). Under these conditions, the reflected beam is purely RHCP.

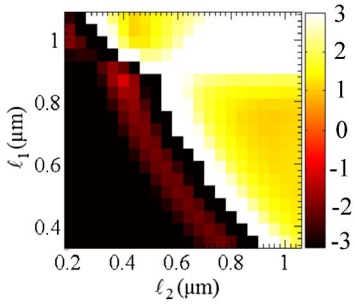

Fig. 4. Axial ratio of the reflected wave from a MS consists of an infinite periodic array of identical Y-shaped nanoantennas as a function of the arm length and the stub length. The arm angle, Δ, is fixed at 50°.

The axial ratio of the reflected wave from a MS made of an infinite periodic array of identical Y-shaped nanoantennas is calculated from Eq. (7) and plotted, as a function of the arm length, ℓ_1, and the stub length, ℓ_2, in Fig. 4. Positive and negative axial ratios define the LHCP and the RHCP waves, respectively. Although the results provided in Figs. 3 and 4 calculated for a specific value of the arm angle ($\Delta = 50°$), similar plots can be obtained for other values of the arm angle. Figure 4 reveals that for arbitrary pairs of the arm length and the arm angle, a proper stub length can be found such that the axial ratio of the reflected wave is positive and its magnitude is less than 1.42 or 3 dB (LHCP).

4. POLARIZING LENS DESIGN

Based on the results and the theory provided in the previous sections, here we show the performance of a designed square, flat, polarizing lens with dimensions 28 μm × 28 μm ($6.51\lambda \times 6.51\lambda$) with focal length $f = 35$ μm, corresponding to a numerical aperture of 0.37. It is supposed to focus an incident beam with oblique incidence of $\alpha = 30°$, shown in Fig. 5(a). The beam waist of the incident Gaussian wave ($w_0 = 25$ μm) is chosen so that almost the entire surface of the polarizing lens is illuminated by a plane-wave-like wavefront. Figure 5 shows the schematic of the simulation setup together with the intensity of the scattered field in the longitudinal and transverse planes at $\lambda = 4.3$ μm, calculated by FEM full wave simulations (provided by HFSS by Ansys Inc.). The focus generated by the MS is clearly observed. The simulation result for the axial ratio of the scattered wave along the y transverse direction, in the focal plane, is plotted in Fig. 5(c). The axial ratio is around 3 dB in the focal region.

The designed polarizing lens preserves good focusing and polarization conversion properties over a relatively broad wavelength range from 3.8 to 4.8 μm. Figure 6 shows the normalized intensity distribution for the scattered field at different incident wavelengths around the central wavelength of 4.3 μm. The axial ratio of the scattered field along a y-directed line passing through the center of the focal spot in the transverse focal plane is shown in Fig. 7. The focal spot slightly shifts in the positive x-direction as the wavelength increases

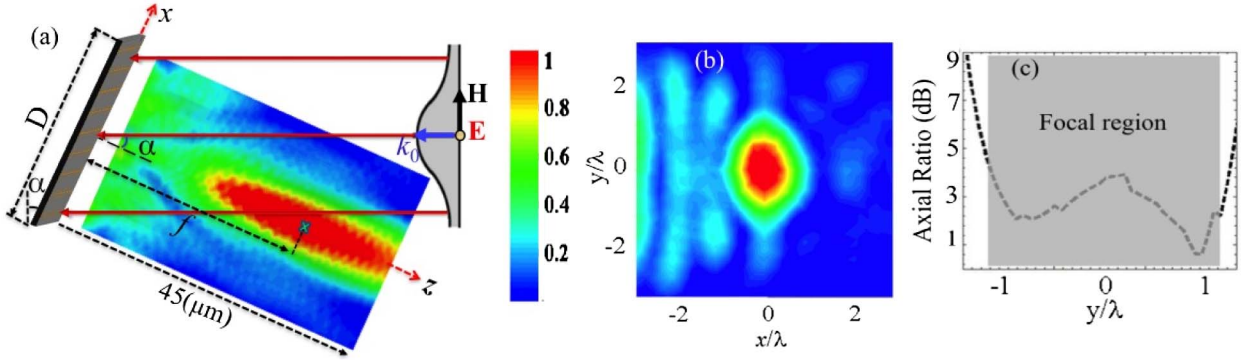

Fig. 5. (a) Simulation setup together with the full wave simulated results of the normalized scattered field intensity ($|\mathbf{E}|^2/|\mathbf{E}_0|^2$) in x–z plane at $\lambda = 4.3$ μm: for a 28 μm by 28 μm sized flat polarizing lens with $f = 35$ μm, and $\alpha = 30°$, (b) the normalized intensity of the scattered field in x–y transverse focal plane. (c) Axial ratio of the scattered wave along a horizontal line in the focal plane ($x = 0, z = 35$ μm). The highlighted rectangle shows the focus region.

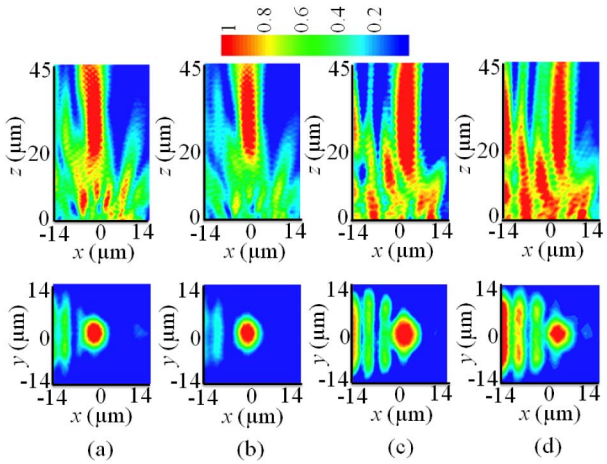

Fig. 6. Full wave simulation results of the normalized scattered electric field intensity in the x–z longitudinal plane (top) and x–y transverse focal plane, $z = 35$ μm (bottom) at operating wavelength of (a) 3.8 μm, (b) 4 μm, (c) 4.6 μm, and (d) 4.8 μm. Each case has been normalized to its own maximum.

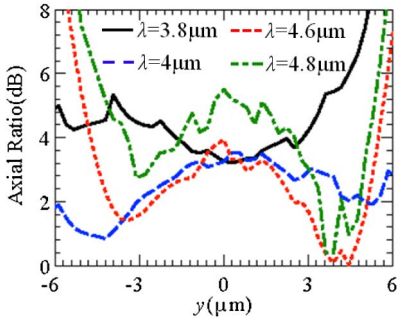

Fig. 7. Axial ratio in the focal plane ($z = 35$ μm) evaluated along the y-directed line passing through the center of the focal spot. The y-directed line is located at $x = -2.5$, -1.5, 1.5, 2.5 μm for wavelengths 3.8, 4, 4.6, and 4.8 μm, respectively.

from 3.8 to 4.8 μm. This lateral chromatic aberration is mainly attributed to the oblique incidence angle of $\alpha = 30°$ [see Fig. 5(a)]. In principle, the extra degree of freedom available in Y-shaped nanoantennas allows also to control the phase and amplitude of the reflection coefficient at other wavelengths than the central one, though this capability should be further investigated and may lead to a better control of chromatic aberration. Figure 8 shows the absorption of the focusing MS, defined as the ratio of the power loss in the MS to the total power illuminating it, versus wavelength. The power lost in the MS is calculated by integrating $\omega\varepsilon''|\mathbf{E}|^2/2$ over the whole metal volume of the Y-nanoantennas, substrate and ground plane, where ε'' is the imaginary part of the respective material permittivity. Absorption peaks at $\lambda = 4.3$ μm and it is less than 0.36 over a broadband wavelength ranging from 3.8 to 4.8 μm.

Optical paths from nanoantennas at or close to the edge of the MS to the focal point differ significantly even between neighboring nanoantennas. This requires a large variation of nanoantenna dimensions between neighboring nanoantennas located at or close to the edges [9] to guarantee focusing. Moreover, nanoantennas at the MS edges are not surrounded by other nanoantennas on all sides. Therefore the local

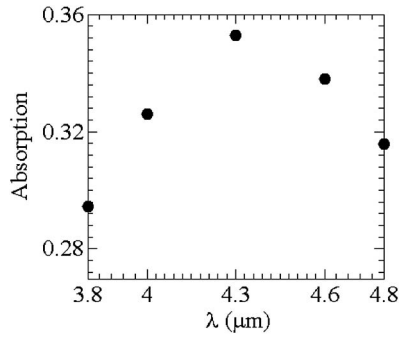

Fig. 8. Absorption of the MS-based polarizing lens versus wavelength. Absorption is defined as the power lost in the reflecting MS normalized by the incident power upon the MS.

periodicity assumption discussed earlier in this paper is invalid for those nanoantennas [9]; as a result, the simulated reflection coefficients used to establish focusing may not model the scattering from these nanoantennas accurately. However, these edge-nanoantennas constitute only a small percentage of the total number of nanoantennas in the MS and their inaccurate modeling does not cause a significant change in the focusing field properties [9]. Increasing the size of the MS not only reduces the effect of undesirable MS edge diffraction on both focusing and polarization conversion but also increases the number of the nanoantennas for which the local periodicity assumption used in the design process is accurate [9]. Larger MSs would improve the polarizing lens performance and result in finer focus spots with smaller axial ratio.

5. CONCLUSION

The concept and design procedure of a flat polarizing lens, capable of simultaneous polarization and focusing manipulation, based on a flat MS is demonstrated in the presence of nonnegligible losses. For this purpose, a planar array of anisotropic Y-shaped nanoantennas is employed to generate light focusing and polarization state conversion because it provides enough degrees of freedom to balance the losses experienced with orthogonal polarizations. Indeed, the Y-shaped nanoantenna allows for the independent tuning of the phases of both x- and y-pol. reflected fields, and at the same time compensate for the natural changes of the magnitude of the reflection coefficient due to losses, which eventually is important to improve the quality of the polarizing lens. The integration of polarizer and lens into a single thin MS layer may have an impact on significantly reducing cost, volume, optical loss, and system complexity.

ACKNOWLEDGMENTS

The authors are grateful to ANSYS, Inc., for providing HFSS that was instrumental in the design. This work was supported in part by the National Science Foundation under NSF Award No. ECCS-1028727.

REFERENCES

1. Z. Bomzon, G. Biener, V. Kleiner, and E. Hasman, "Space-variant pancharatnam-berry phase optical elements with computer-generated subwavelength gratings," Opt. Lett. **27**, 1141–1143 (2002).
2. Z. Bomzon, G. Biener, V. Kleiner, and E. Hasman, "Radially and azimuthally polarized beams generated by space-variant dielectric subwavelength gratings," Opt. Lett. **27**, 285–287 (2002).

3. N. Yu, P. Genevet, M. A. Kats, F. Aieta, J. Tetienne, F. Capasso, and Z. Gaburro, "Light propagation with phase discontinuities: generalized laws of reflection and refraction," Science **334**, 333–337 (2011).
4. X. Ni, N. K. Emani, A. V. Kildishev, A. Boltasseva, and V. M. Shalaev, "Broadband light bending with plasmonic nanoantennas," Science **335**, 427 (2012).
5. A. V. Kildishev, A. Boltasseva, and V. M. Shalaev, "Planar photonics with metasurfaces," Science **339**, 1232009 (2013).
6. F. Monticone, N. Estakhri, and A. Alu, "Full control of nanoscale optical transmission with a composite metascreen," Phys. Rev. Lett. **110**, 203903 (2013).
7. N. Yu and F. Capasso, "Flat optics with designer metasurfaces," Nat. Mater. **13**, 139–150 (2014).
8. F. Aieta, P. Genevet, N. Yu, M. A. Kats, Z. Gaburro, and F. Capasso, "Out-of-plane reflection and refraction of light by anisotropic optical antenna metasurfaces with phase discontinuities," Nano Lett. **12**, 1702–1706 (2012).
9. J. Huang and J. A. Encinar, *Reflectarray Antennas*, 1st ed. (Wiley, 2008).
10. F. Aieta, P. Genevet, M. A. Kats, N. Yu, R. Blanchard, Z. Gaburro, and F. Capasso, "Aberration-free ultrathin flat lenses and axicons at telecom wavelengths based on plasmonic metasurfaces," Nano Lett. **12**, 4932–4936 (2012).
11. X. Ni, S. Ishii, A. V. Kildishev, and V. M. Shalaev, "Ultra-thin, planar, Babinet-inverted plasmonic metalenses," Light Sci. Appl. **2**, e27 (2013).
12. A. Pors, M. G. Nielsen, R. L. Eriksen, and S. I. Bozhevolnyi, "Broadband focusing flat mirrors based on plasmonic gradient metasurfaces," Nano Lett. **13**, 829–834 (2013).
13. X. Li, S. Xiao, B. Cai, Q. He, T. J. Cui, and L. Zhou, "Flat metasurfaces to focus electromagnetic waves in reflection geometry," Opt. Lett. **37**, 4940–4942 (2012).
14. B. Memarzadeh and H. Mosallaei, "Array of planar plasmonic scatterers functioning as light concentrator," Opt. Lett. **36**, 2569–2571 (2011).
15. X. Chen, L. Huang, H. Mühlenbernd, G. Li, B. Bai, Q. Tan, G. Jin, C. Qiu, S. Zhang, and T. Zentgraf, "Dual-polarity plasmonic metalens for visible light," Nat. Commun. **3**, 1198–1203 (2012).
16. Y. Zhao and A. Alu, "Manipulating light polarization with ultrathin plasmonic metasurfaces," Phys. Rev. B **84**, 205428 (2011).
17. F. Wang, A. Chakrabarty, F. Minkowski, K. Sun, and Q. Wei, "Polarization conversion with elliptical patch nanoantennas," Appl. Phys. Lett. **101**, 023101 (2012).
18. N. Yu, F. Aieta, P. Genevet, M. A. Kats, Z. Gaburro, and F. Capasso, "A broadband, background-free quarter-wave plate based on plasmonic metasurface," Nano Lett. **12**, 6328–6333 (2012).
19. M. Farmahini Farahani and H. Mosallaei, "A birefringent reflectarray metasurface for beam engineering in infrared," Opt. Lett. **38**, 462–464 (2013).
20. C. Pfeiffer and A. Grbic, "Cascaded metasurfaces for complete phase and polarization control," Appl. Phys. Lett. **102**, 231116 (2013).
21. A. Pors and S. I. Bozhevolnyi, "Plasmonic metasurfaces for efficient phase control in reflection," Opt. Express **21**, 27438–27451 (2013).
22. D. L. Markovich, A. Andryieuski, M. Zalkovskij, R. Malureanu, and A. V. Lavrinenko, "Metamaterial polarization converter analysis: limits of performance," Appl. Phys. B **112**, 143–152 (2013).
23. M. Joyal and J. Laurin, "Analysis and design of thin circular polarizers based on meander lines," IEEE Trans. Antennas Propag. **60**, 3007–3011 (2012).
24. C. Pfeiffer and A. Grbic, "Millimeter-wave transmitarrays for wavefront and polarization control," IEEE Trans. Microwave Theory Tech. **61**, 4407–4417 (2013).
25. E. Carrasco and J. Perruisseau-Carrier, "Reflectarray antenna at terahertz using grapheme," IEEE Antennas Wireless Propag. Lett. **12**, 253–256 (2013).
26. A. D. Rakić, A. B. Djurišic, J. M. Elazar, and M. L. Majewski, "Optical properties of metallic films for vertical-cavity optoelectronic devices," Appl. Opt. **37**, 5271–5283 (1998).
27. R. Kitamura, L. Pilon, and M. Jonasz, "Optical constants of silica glass from extreme ultraviolet to far infrared at near room temperature," Appl. Opt. **46**, 8118–8133 (2007).
28. M. A. Kats, R. Blanchard, P. Genevet, Z. Yang, M. Qazilbash, D. N. Basov, S. Ramanathan, and F. Capasso, "Thermal tuning of mid-infrared plasmonic antenna arrays using a phase change material," Opt. Lett. **38**, 368–370 (2013).
29. C. A. Balanis, *Advanced Engineering Electromagnetics* (Wiley, 1989).